

See discussions, stats, and author profiles for this publication at: <https://www.researchgate.net/publication/240487997>

Empirical cotidal charts of the Bohai, Yellow, and East China Seas from 10 years of TOPEX/Poseidon altimetry

Article in *Journal of Geophysical Research Atmospheres* · November 2004

DOI: 10.1029/2004JC002484

CITATIONS

69

READS

122

6 authors, including:



[Guohong Fang](#)

First Institute of Oceanography

82 PUBLICATIONS 1,624 CITATIONS

[SEE PROFILE](#)



[Yonggang Wang](#)

First Institute of Oceanography

27 PUBLICATIONS 338 CITATIONS

[SEE PROFILE](#)



[Zexun Wei](#)

First Institute of Oceanography

57 PUBLICATIONS 628 CITATIONS

[SEE PROFILE](#)



[Xinyi Wang](#)

UNSW Sydney

88 PUBLICATIONS 571 CITATIONS

[SEE PROFILE](#)

Empirical cotidal charts of the Bohai, Yellow, and East China Seas from 10 years of TOPEX/Poseidon altimetry

Guohong Fang,^{1,2} Yonggang Wang,^{1,2,3} Zexun Wei,^{1,2} Byung Ho Choi,⁴ Xinyi Wang,^{1,2} and Ji Wang⁵

Received 13 May 2004; revised 29 July 2004; accepted 13 August 2004; published 10 November 2004.

[1] Harmonic analysis of 10 years of TOPEX/Poseidon (TP) along-track altimetry is performed to derive the semidiurnal, diurnal, long-period, and quarter-diurnal tides in the Bohai, Yellow, and East China Seas. The TP solutions are evaluated through intercomparison for crossover points and comparison with the ground truth, showing that the accuracy of TP solutions in the study area has achieved levels of 2–4 cm in amplitudes and 5° in phase lags for principal constituents (M_2 , S_2 , K_1 , O_1 , and S_a). The TP-derived S_a amplitudes have a systematic bias of about –10% as compared with the ground truth, indicating the possible importance of loading effect of this constituent in the study area, which is generally not considered in geodetic surveys. The tidal harmonics from TP altimetry and at coastal and island stations are used to give a new set of empirical cotidal charts for principal constituents (M_2 , S_2 , K_1 , O_1 , and S_a). The accuracy of these new charts is believed to be significantly higher than the previous charts for the offshore area. **INDEX TERMS:** 1255 Geodesy and Gravity: Tides—ocean (4560); 4556 Oceanography: Physical: Sea level variations; 4275 Oceanography: General: Remote sensing and electromagnetic processes (0689); 4223 Oceanography: General: Descriptive and regional oceanography; **KEYWORDS:** cotidal charts, Bohai, Yellow and East China Seas, TOPEX/Poseidon altimetry

Citation: Fang, G., Y. Wang, Z. Wei, B. H. Choi, X. Wang, and J. Wang (2004), Empirical cotidal charts of the Bohai, Yellow, and East China Seas from 10 years of TOPEX/Poseidon altimetry, *J. Geophys. Res.*, 109, C11006, doi:10.1029/2004JC002484.

1. Introduction

[2] The Bohai, Yellow, and East China Seas are shallow except the narrow Okinawa Trough near the Ryukyu Islands (Figure 1). The tidal regime in this area is quite complicated and the tidal ranges are relatively large. Before the satellite altimeter data became available, the cotidal charts for the area were drawn empirically on the basis of observations at coastal and island tidal gauge stations [Ogura, 1933; Fang, 1986], or constructed on the basis of numerical simulations [Choi, 1980; Fang and Yang, 1985; Choi and Fang, 1993; Zhao *et al.*, 1993; Kang *et al.*, 1998; Lee and Jung, 1999; Lefevre *et al.*, 2000]. TOPEX/Poseidon (TP) altimeter data were first employed by Mazzega and Berge [1994] to derive ocean tides in the East Asian marginal seas. In their study only

the data of cycles 2 to 22 (covering about 7 months) were used while the basic patterns of tidal regimes were obtained. Yanagi *et al.* [1997] used TOPEX data from cycle 1 to 108, covering about 3 years, to construct cotidal charts for the Yellow and East China Seas, showing significant improvement over Mazzega and Berge's solution. Teague *et al.* [2000] evaluated the tides in the Bohai and Yellow Seas derived from 5 years of TP measurements. Fairly good agreement with the coastal and offshore gauge measurements was achieved. Now 10 years of TP altimeter data have become available to users. The increased length of measurement greatly improves the separation between K_1 and S_{sa} and between P_1 and K_2 , and therefore enables us to derive more accurate tidal harmonic constants.

[3] In the present study, we use 10 years of TP altimeter data from the beginning of the TP mission in September 1992 to the completion of the calibration/validation phase of the Jason mission in September 2002, then TP was moved to a parallel orbit halfway between its previous repeat tracks. The conventional harmonic method is employed to analyze the TP-measured data at each selected point along the tracks (Figure 2). To evaluate the accuracy of the obtained tidal harmonics, we gather as much as possible harmonic constants derived from tide gauge measurements at island and offshore stations. The intercomparison between results at crossover points and comparison to the gauge data are made to show the

¹First Institute of Oceanography, State Oceanic Administration, Qingdao, China.

²Also at Key Lab of Marine Science and Numerical Modeling, State Oceanic Administration, Qingdao, China.

³Also at Institute of Oceanology, Chinese Academy of Sciences, Qingdao, China.

⁴Department of Civil and Environment Engineering, Sungkyunkwan University, Suwon, Korea.

⁵National Marine Data and Information Service, Tianjin, China.

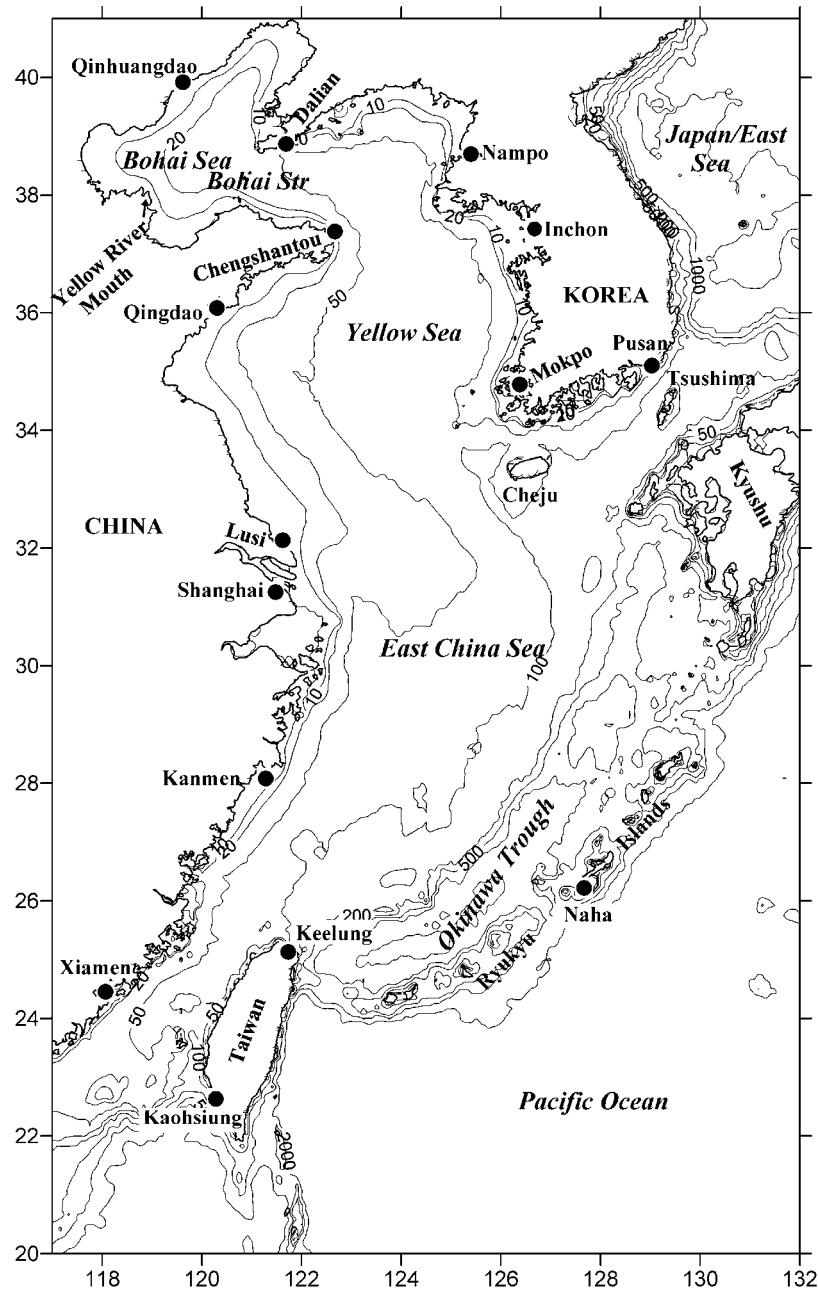


Figure 1. Map of the Bohai, Yellow, and East China Seas. Bathymetry contours are given in meters.

reliability of the TP solution. On the basis of TP solution and tidal gauge results, new cotidal charts for principal constituents are given.

2. Methods

[4] To extract ocean tides, we use TP-measured sea surface heights relative to the solid earth surface:

$$h = \text{SSH} - \text{MSSH} - \text{SET} - \text{LT} - \text{PT}, \quad (1)$$

where SSH represents the sea surface height above the reference ellipsoid, MSSH the mean ocean surface, SET the solid earth tide, LT the loading tide, and PT the pole tide.

The data were provided by Jet Propulsion Laboratory in MGDR-B [Benada, 1997].

[5] In addition to the crossover points, we select 15 equally spaced points between each pair of neighboring crossover points along each track. The TP measured heights are linearly interpolated to these fixed points. The valid records at these points are used in the harmonic analysis, in which the conventional tidal function is employed to fit the interpolated heights:

$$\hat{h} = H_0 + \sum_i f_i H_i \cos[\omega_i t + (V_i + u_i) - g_i], \quad (2)$$

where H_0 is the mean height, H the amplitude, g the phase lag, ω the angular speed, f the nodal factor, $V + u$ the initial phase of the equilibrium tide with u repre-

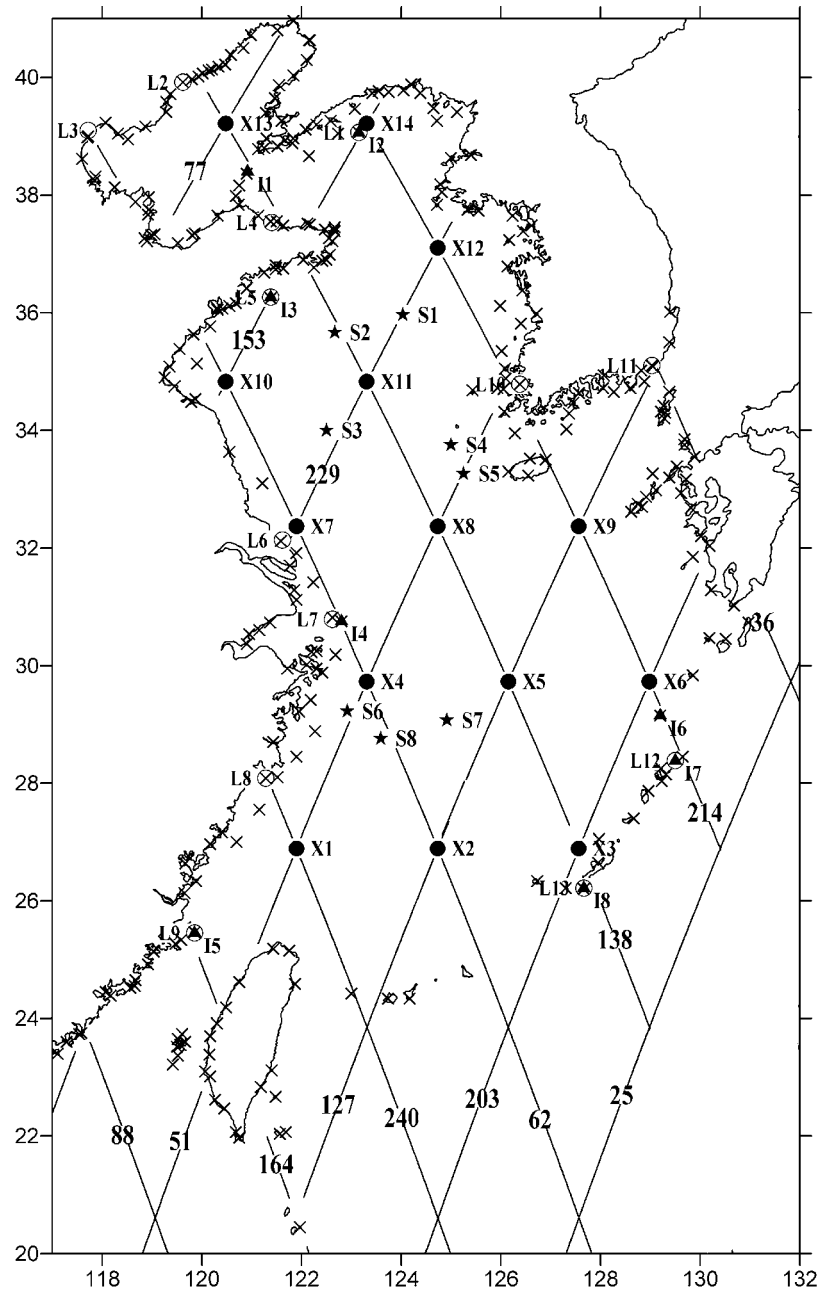


Figure 2. TOPEX/Poseidon ground tracks, crossover points, and ground tidal stations. X1–X14 are TP crossover points; I1–I8 island tidal stations; S1–S8 open sea tidal stations; and L1–L11 long-term tidal stations. Intercomparison of the TP solutions on ascending and descending tracks is made for the crossover points. The harmonics at island and open sea stations are used to evaluate the TP solutions of M_2 , S_2 , K_1 , and O_1 . The harmonics at long-term stations are used to evaluate the TP solution of S_a . Crosses are coastal and island stations where the harmonic constants are used in mapping cotidal charts.

senting nodal adjustment angle of the initial phase. The subscript i in (2) represents the constituents considered in the analysis, as listed in Table 1. The least squares fitting yields the harmonic constants H_i and g_i [cf. *Godin, 1972; Foreman, 1977; Fang et al., 1986; Pawlowicz et al., 2002*].

[6] In the analysis of altimeter data the aliasing effect must be considered [*Schlax and Chelton, 1994*]. At a fixed

subsattellite point the sea surface heights are sampled at a time interval Δt , which is equal to orbital repeat period of the satellite. The Nyquist critical frequency corresponding to the sampling interval Δt is

$$f_c = 1/(2\Delta t). \quad (3)$$

Table 1. Tidal Periods and TP Alias Periods

Constituent	Tidal Period, days	Alias Period, days
S _a	365.24220	365.24220
S _{sa}	182.62110	182.62110
Q ₁	1.1195149	69.38300
O ₁	1.0758059	45.70615
P ₁	1.0027454	88.92464
K ₁	0.9972696	173.32047
N ₂	0.5274312	49.54809
M ₂	0.5175251	62.07619
S ₂	0.5000000	58.77120
K ₂	0.4986348	86.66024
M ₄	0.2587625	31.03810
MS ₄	0.2543058	1103.87327

A tidal constituent of frequency f may have a number of alias frequencies as follows [cf. *Godin, 1972; Fang et al., 1986*]:

$$f_a(m) = 2mf_c \pm f, \quad m = 0, 1, 2, \dots \quad (4)$$

Among these frequencies only the lowest one falls into the range $[-f_c, f_c]$ and is of concern to us. This particular alias frequency can be calculated from the formula

$$f_a = \min|2mf_c - f|, \quad m = 0, 1, 2, \dots \quad (5)$$

Previously the repeat period of TP orbit was generally taken to be 9.9156 days [*Fu et al., 1994; Schlax and Chelton, 1994*]. In the present study we will use a more precise repeat period of 9.9156420 days, which can be readily calculated from the sampling times in TP records. The corresponding Nyquist critical frequency is equal to $0.050425378 \text{ d}^{-1}$. From this value we get the alias periods for each constituent as shown in Table 1. The periods of the constituents S_a and S_{sa} are longer than twice the TP repeat period, thus no aliasing is induced. We simply use original periods for their alias periods in the table.

[7] To fully resolve two constituents of alias frequencies f_{a1} and f_{a2} , the measurement time span T must satisfy the Rayleigh criterion, that is

$$T \geq T_s, \quad (6)$$

where

$$T_s = 1/|f_{a1} - f_{a2}| \quad (7)$$

represents the time span required for the phase difference between the associated two constituents to reach 1 cycle, and is thus called their alias synodic period. The TP alias synodic periods of each pair of constituents are listed in Table 2.

[8] We can see from Table 2 that among these 11 constituents the longest TP alias synodic period is 9.32 years. Therefore the data length in the present study is sufficient for resolving all constituents listed in Table 1. However, it should be mentioned here that the alias period of MS₄ is about 3 years, which corresponds to the periods of active oceanic interannual variabilities, such as El Nino events. Thus the interannual oceanic variabilities may contaminate the TP-derived MS₄ harmonics. Another issue of certain importance is that, a satellite constituent of K₁ with period equal to 1.0028850 days and amplitude approximately equal to 14% of K₁ has an alias period of 177.85514 days. The alias synodic period of this satellite constituent and S_{sa} is 18.66 years, which is about twice the length of existing TP data. Thus the error induced from the given nodal factor of K₁ will be transferred to the constituent S_{sa}. Likewise, the error in the nodal factor of K₂ will also yield error in the computed P₁.

[9] The TP measurements along the ground tracks passing the Bohai, Yellow, and East China Seas can be analyzed through the least squares fit to produce harmonic constants as described above. Figure 2 shows the position of the tracks. No. 88, 164, 240, 62, 138, 214 and 36 are descending tracks and No. 77, 153, 229, 51, 127, 203 and 25 are ascending tracks. The crossover points are indicated by solid dots. The positions of the ground measurement sites for validating TP solutions are indicated by stars, triangles and open circles. The stars and triangles indicate offshore and island gauge stations where the diurnal and semidiurnal harmonics are available. The open circles indicate long-term coastal or island tidal stations where annual and semiannual harmonics will be used for comparison.

3. Evaluation of Harmonics Derived From TP Altimeter Data

3.1. Intercomparison of TP-Derived Harmonics at Crossover Points

[10] There are in total 14 crossover points within the study area, indicated by solid dots and numbered with X1, X2, ..., X14 in Figure 2. The comparison is shown in Tables 3a–3c, in which H represents the amplitude derived from both the ascending and descending records, Δ is the

Table 2. TP Alias Synodic Periods of Each Pair of Constituents (in years)

	S _{sa} , years	Q ₁ , years	O ₁ , years	P ₁ , years	K ₁ , years	N ₂ , years	M ₂ , years	S ₂ , years	K ₂ , years	M ₄ , years	MS ₄ , years
S _a	1.000	0.235	0.143	0.322	0.903	0.157	0.205	0.192	0.311	0.093	1.495
S _{sa}		0.306	0.167	0.475	9.317	0.186	0.257	0.237	0.452	0.102	0.599
Q ₁			0.367	0.864	0.317	0.475	1.614	1.052	0.953	0.154	0.203
O ₁				0.257	0.170	1.614	0.475	0.563	0.265	0.265	0.131
P ₁					0.500	0.306	0.563	0.475	9.317	0.131	0.265
K ₁						0.190	0.265	0.243	0.475	0.104	0.563
N ₂							0.672	0.864	0.317	0.227	0.142
M ₂								3.022	0.599	0.170	0.180
S ₂									0.500	0.180	0.170
K ₂										0.132	0.257
M ₄											0.087

Table 3a. Difference Between Harmonics Derived From Ascending and Descending Passes at Crossover Points: Semidiurnal Constituents

	Location, °N, °E	M_2		S_2		N_2		K_2	
		H	Δ	H	Δ	H	Δ	H	Δ
X1	26.89, 121.90	112.15	2.02	38.09	2.15	21.15	1.35	10.59	3.49
X2	26.89, 124.73	58.95	0.10	23.15	0.99	11.32	1.59	7.34	1.80
X3	26.89, 127.56	56.40	1.27	24.04	1.67	11.05	0.54	6.81	1.63
X4	29.73, 123.31	118.40	2.10	51.15	0.94	21.15	0.38	14.43	2.43
X5	29.73, 126.15	70.20	1.58	29.15	0.71	13.50	1.03	8.54	1.67
X6	29.73, 128.98	56.19	3.26	25.85	3.85	10.69	1.09	6.14	0.95
X7	32.37, 121.90	151.39	7.48	64.68	10.18	28.80	0.94	18.64	4.30
X8	32.37, 124.73	69.50	0.60	31.69	2.17	14.65	0.75	9.00	2.87
X9	32.37, 127.56	67.20	1.83	30.05	0.50	13.54	1.91	8.25	0.33
X10	34.83, 120.48	80.50	1.72	18.91	2.65	15.47	2.75	5.26	1.63
X11	34.83, 123.31	63.45	1.15	22.29	1.31	11.90	0.65	6.05	0.82
X12	37.10, 124.73	102.95	2.90	40.89	2.46	19.24	1.35	12.07	1.69
X13	39.22, 120.48	26.56	5.72	10.97	1.83	3.26	1.64	3.30	0.85
X14	39.22, 123.31	151.94	7.21	48.30	6.46	29.93	2.09	16.64	7.62
RMS		92.00	3.59	35.63	3.71	17.58	1.44	10.44	2.92

vectorial difference between the ascending and descending solutions, defined by

$$\Delta = \left[(H_a \cos g_a - H_d \cos g_d)^2 + (H_a \sin g_a - H_d \sin g_d)^2 \right]^{1/2}, \quad (8)$$

where the subscriptions a and d represent ascending and descending solutions respectively.

[11] From Tables 3a–3c we see that the RMS differences are more or less independent of frequency, with a maximum of 3.7 cm for S_2 and a minimum of 1.44 cm for N_2 . Averaged difference of all constituents is 2.4 cm. The next largest RMS difference is M_2 , 3.6 cm. Since M_2 itself is the largest constituent for the area, it is understandable that the derived M_2 harmonics contain relatively greater error because of greater spectral cusp surrounding M_2 [Munk *et al.*, 1965]. However, it is worth noticing that the relative RMS difference of M_2 is the smallest (0.04). The relative RMS differences of S_{sa} and MS_4 are greater than one, that is, the RMS differences of these constituents are greater than the RMS amplitudes themselves. This indicates that the harmonics of these constituents obtained from harmonic analysis are not representative for the true values. The relative RMS differences of Q_1 and M_4 are smaller than 1 but

exceed 0.5. Thus only in some individual areas the derived harmonics are of significance. For example, the derived harmonics of Q_1 are still useful for the area remote from the shore, such as at crossover points X1, X2, X3, X5, X6 and X9. For M_4 constituent, only in the areas where the shallow water tides are important, e.g. at the crossover points X4 and X10, the derived harmonics are of certain significance.

3.2. TP-Ground Comparison for Diurnal and Semidiurnal Tides

[12] The in situ sea surface height observations are sparse in the open sea of the study area. The tidal harmonic constants of 4 principal constituents at 8 open sea stations are available to us (S1–S8 in Figure 2). Among these stations, the observations at stations S1, S4 and S5 were carried by Teague *et al.* [1998] and were used for comparison with TP solutions by Teague *et al.* [2000]. The measurements at the remaining 5 stations were carried out by Chinese oceanographers for the purpose of offshore oil platform/pipeline design. The harmonic constants obtained from ground observation and interpolated from TP solutions are listed in Table 4. In general, the agreement between the harmonics derived from ground and TP measurements is satisfactory. The RMS differences in amplitudes of M_2 , S_2 , K_1 , and O_1 are 4.8, 2.2, 1.4 and 1.7 cm, respectively; those

Table 3b. Differences Between Harmonics Derived From Ascending and Descending Passes at Crossover Points: Diurnal Constituents

	Location, °N, °E	K_1		O_1		P_1		Q_1	
		H	Δ	H	Δ	H	Δ	H	Δ
X1	26.89, 121.90	26.15	2.47	19.35	1.73	7.44	4.69	3.49	0.74
X2	26.89, 124.73	22.20	0.39	17.05	0.92	7.14	0.80	3.79	0.56
X3	26.89, 127.56	19.79	1.60	16.94	0.94	6.14	0.65	3.10	0.64
X4	29.73, 123.31	26.70	1.68	19.60	1.20	8.38	3.88	2.66	4.33
X5	29.73, 126.15	23.05	1.36	16.85	2.57	6.94	0.88	3.97	1.05
X6	29.73, 128.98	22.71	2.92	17.98	1.98	7.36	2.22	3.84	1.40
X7	32.37, 121.90	18.69	1.00	9.75	4.88	7.26	1.58	1.33	2.58
X8	32.37, 124.73	18.96	2.33	13.75	1.77	5.68	2.77	3.02	1.60
X9	32.37, 127.56	23.14	1.62	16.55	0.30	7.90	1.50	3.65	0.98
X10	34.83, 120.48	23.49	3.79	18.25	0.64	5.64	3.81	4.61	3.03
X11	34.83, 123.31	8.06	1.66	8.39	1.16	2.52	1.86	2.29	2.28
X12	37.10, 124.73	30.05	1.26	21.84	1.25	8.88	2.20	4.27	1.80
X13	39.22, 120.48	21.59	1.39	16.10	0.34	6.64	2.02	2.79	3.50
X14	39.22, 123.31	33.85	5.90	22.90	4.47	10.54	1.05	2.67	3.68
RMS		23.46	2.49	17.25	2.19	7.25	2.45	3.36	2.34

Table 3c. Differences Between Harmonics Derived From Ascending and Descending Passes at Crossover Points: Annual, Semiannual, and Quarter-Diurnal Constituents

	Location, °N, °E	S_a		S_{sa}		M_4		MS_4	
		H	Δ	H	Δ	H	Δ	H	Δ
X1	26.89, 121.90	16.14	1.55	1.48	0.44	0.11	1.20	0.90	1.74
X2	26.89, 124.73	13.10	0.50	2.35	0.90	0.33	0.48	0.65	0.34
X3	26.89, 127.56	13.00	1.38	2.85	0.56	0.58	0.92	3.16	1.13
X4	29.73, 123.31	15.15	0.90	1.88	0.84	3.25	0.96	2.55	1.46
X5	29.73, 126.15	16.45	0.42	1.49	0.58	2.47	1.62	1.81	2.38
X6	29.73, 128.98	16.55	0.76	0.49	0.20	1.02	2.59	0.99	2.47
X7	32.37, 121.90	16.20	1.04	3.12	2.94	1.47	4.10	2.52	5.06
X8	32.37, 124.73	17.74	0.93	1.67	1.66	2.74	1.26	2.43	1.90
X9	32.37, 127.56	16.05	0.75	2.10	0.41	1.84	2.99	1.05	0.96
X10	34.83, 120.48	19.24	2.17	3.78	2.54	6.15	1.52	3.07	2.90
X11	34.83, 123.31	15.04	1.05	1.30	1.00	3.78	1.40	1.94	0.99
X12	37.10, 124.73	16.91	2.91	2.39	2.15	1.34	1.00	1.16	1.52
X13	39.22, 120.48	25.15	0.50	1.91	6.12	1.24	0.78	2.45	1.74
X14	39.22, 123.31	21.40	4.16	1.20	6.51	3.09	3.14	5.22	5.20
RMS		17.28	1.70	2.16	2.75	2.62	2.00	2.44	2.54

in phase lags are 8.4° , 11.0° , 26.3° , and 28.0° , respectively. The greatest phase deviations of K_1 and O_1 appear at station S3, which is close to the amphidromic points of the diurnal tides. When this station is excluded in the statistics, the corresponding phase RMS differences of K_1 and O_1 become 9.5° and 7.0° , respectively, which are given in the parentheses in Table 4.

[13] Several islands in the study area are quite close to the subsatellite tracks. Harmonic constants at 8 islands (I1–I8 in Figure 2) are used for comparison with TP solutions. The comparison is shown in Table 5. The RMS differences in amplitudes of M_2 , S_2 , K_1 and O_1 are 2.4, 1.9, 1.8 and 1.7 cm, respectively, and those in phase lags are 5.5° , 5.1° , 5.0° and 4.5° , respectively.

[14] The deviations between TP and open sea gauge results are larger than those between TP and island gauge results. This can be attributed to the greater errors in the open sea results, due to greater instrument noise and shorter duration of measurements.

3.3. TP-Ground Comparison for the Annual Constituent S_a

[15] The seasonal variations of sea level are important in the Bohai, Yellow, and East China Seas. These variations are generally represented by S_a and S_{sa} constituents, which are actually of meteorological (or solar radiational) origin. To obtain reliable harmonic constants for these constituents, sea level observation of at least several years is necessary.

Table 4. Comparison Between TP-Measured and Ground-Measured Harmonics at Offshore Stations^a

	Station	N/E	Duration	amp/pha	M ₂	S ₂	K ₁	O ₁
S1	TPHJ-C	35.97/124.03	4.5 months	H/g(gr)	88.4/41.2	30.3/89.8	20.3/281.7	16.6/243.0
				H/g(TP)	87.6/55.0	30.8/106.0	20.2/287.0	15.8/248.0
				ΔH/Δg	−0.8/13.8	0.5/16.2	0.1/5.3	−0.8/5.0
S2	F-1	35.67/122.67	1.2 months	H/g(gr)	59.0/58.0	23.0/105.0	16.0/304.0	16.0/283.0
				H/g(TP)	61.1/49.0	22.3/95.0	15.3/328.0	12.7/278.0
				ΔH/Δg	2.1/−9.0	−0.7/−10.0	−0.7/24.0	−3.3/−5.0
S3	F-2	34.00/122.50	22 days	H/g(gr)	77.0/340.0	29.0/13.0	7.0/150.0	5.0/244.0
				H/g(TP)	79.3/333.0	29.2/17.0	5.7/80.0	4.4/321.0
				ΔH/Δg	2.3/−7.0	0.2/4.0	−1.3/−70.0	−0.6/77.0
S4	TPHJ-B	33.75/125.00	4.1 months	H/g(gr)	70.2/327.8	23.6/354.0	18.9/215.0	13.6/186.8
				H/g(TP)	69.0/333.0	24.2/5.0	18.1/216.0	12.2/186.0
				ΔH/Δg	−1.2/5.2	0.6/11.0	−0.8/1.0	−1.4/−0.8
S5	TPHJ-A	33.27/125.25	4.1 months	H/g(gr)	64.7/303.4	24.8/326.1	20.5/206.5	14.5/177.0
				H/g(TP)	66.8/311.0	26.6/341.0	19.6/211.0	13.6/181.0
				ΔH/Δg	2.1/7.6	1.8/14.9	−0.9/4.5	−0.9/4.0
S6	PH-4	29.23/122.92	7 days	H/g(gr)	130.1/247.2	52.5/287.8	28.8/204.8	19.5/162.9
				H/g(TP)	132.1/247.0	55.1/291.0	27.9/205.0	20.8/170.0
				ΔH/Δg	2.0/−0.2	2.6/3.2	−0.9/0.2	1.3/7.1
S7	PH-7	29.07/124.91	1.7 months	H/g(gr)	100.9/217.5	41.1/255.5	27.4/200.7	19.1/161.6
				H/g(TP)	89.3/230.0	36.4/271.0	24.0/205.0	17.0/173.0
				ΔH/Δg	−11.6/12.5	−4.7/15.5	3.4/4.3	−2.1/11.4
S8	PH-5	28.76/123.59	10 days	H/g(gr)	117.4/238.8	47.6/278.2	26.4/205.2	18.1/165.2
				H/g(TP)	112.0/237.0	45.5/279.0	25.7/207.0	19.2/174.0
				ΔH/Δg	−5.4/−1.8	2.1/0.8	−0.7/1.8	1.1/8.8
RMS				σ(H)/σ(g)	4.8/8.4	2.2/11.0	1.4/26.3 (7.0)	1.7/28.0 (9.5)

^aDuration, the record length of ground measurement; amp, amplitude (in cm); pha, phase lag (in degrees, referred to the Beijing standard time); gr, ground measurement; $\Delta H = H(\text{TP}) - H(\text{gr})$; $\Delta g = g(\text{TP}) - g(\text{gr})$; and $\sigma(H)$ and $\sigma(g)$, root mean square values of ΔH and Δg . The RMS values of K_1 and O_1 phase differences in parentheses are statistics with the station S3 excluded.

Table 5. Comparison Between TP-Measured and Ground-Measured Harmonics at Island Stations^a

	Station	N/E	Duration	amp/pha	M ₂	S ₂	K ₁	O ₁
I1	Beihuangcheng	38.40/120.92	1 month	H/g(gr)	59.1/303.2	18.6/358.1	7.2/20.2	4.5/10.4
				H/g(TP)	61.4/292.0	22.6/352.0	9.9/24.0	6.1/8.0
				$\Delta H/\Delta g$	2.3/−11.2	4.0/−6.1	2.7/3.8	1.6/−2.4
I2	Haiyangdao	39.07/123.15	5 years	H/g(gr)	126.3/249.5	41.3/300.5	33.2/335.9	22.9/294.7
				H/g(TP)	128.6/246.0	40.3/298.0	30.5/334.0	20.2/296.0
				$\Delta H/\Delta g$	2.3/−3.5	−1.0/−2.5	−2.7/−1.9	−2.7/1.3
I3	Qianliyan	36.27/121.38	4.6 years	H/g(gr)	98.3/96.1	34.7/139.5	22.3/342.0	18.3/286.1
				H/g(TP)	97.7/98.0	35.3/140.0	21.6/337.0	16.3/279.0
				$\Delta H/\Delta g$	−0.6/1.9	0.6/0.5	−0.7/−5.0	−2.01/−7.1
I4	Shengshan	30.75/122.80	2 months	H/g(gr)	112.7/279.0	52.4/324.4	25.3/195.7	16.5/151.1
				H/g(TP)	108.1/282.0	51.2/328.0	25.7/189.0	17.2/152.0
				$\Delta H/\Delta g$	−4.6/3.0	−1.2/3.6	0.4/−6.7	0.7/0.9
I5	Pingtan	25.24/119.85	4 years	H/g(gr)	201.4/312.1	60.8354.4	30.8/250.7	25.0/212.3
				H/g(TP)	200.4/311.0	58.0/353.0	30.6/250.0	27.2/213.0
				$\Delta H/\Delta g$	−1.0/−1.1	−2.8/−1.4	−0.2/−0.7	2.2/0.7
I6	TakaraShima	29.15/129.20	15 days	H/g(gr)	56.0/180.0	23.0/209.0	22.0/202.0	15.0/172.0
				H/g(TP)	56.2/174.0	24.6/202.0	22.1/193.0	16.5/165.0
				$\Delta H/\Delta g$	0.2/−6.0	1.6/−7.0	0.1/−9.0	1.5/−7.0
I7	Naze	28.38/129.50	28 years	H/g(gr)	56.6/170.3	24.4/204.7	20.0/194.3	15.2/167.7
				H/g(TP)	53.6/169.0	23.4/199.0	20.6/191.0	15.2/162.0
				$\Delta H/\Delta g$	−3.0/−1.3	−1.0/−5.7	0.6/−3.3	0.0/−5.7
I8	Naha	26.22/127.67	26 years	H/g(gr)	57.3/175.5	24.0/208.0	20.6/203.7	15.8/175.3
				H/g(TP)	55.1/168.0	24.2/200.0	17.5/199.0	14.2/171.0
				$\Delta H/\Delta g$	−2.2/−7.5	0.2/−8.0	−3.1/−4.7	−1.6/−4.3
RMS				$\sigma(H)/\sigma(g)$	2.4/5.5	1.9/5.1	1.8/5.0	1.7/4.5

^aDuration, the record length of ground measurement; amp, amplitude (in cm); pha, phase lag (in degrees, referred to the Beijing standard time); gr, ground measurement; $\Delta H = H(TP) - H(gr)$; $\Delta g = g(TP) - g(gr)$; and $\sigma(H)$ and $\sigma(g)$, root mean square values of ΔH and Δg .

Thus only the harmonic constants at coastal and island stations are selected for validation of TP solution. In the study area the S_{sa} constituent is much smaller than S_a , and the crossover intercomparison has shown that the RMS difference of S_{sa} harmonic constants derived from TP measurements are even larger than the RMS value of amplitudes themselves. The comparison between TP and ground results of S_{sa} also demonstrates poor consistency. So here we only show the comparison for S_a constituent, which is given in Table 6. The RMS differences between TP and ground solutions for amplitude and phase lag are 2.2 cm and 5.3° respectively. From Table 6 we can find that almost all the values of ΔH are negative. The mean value of ΔH is −1.9 cm, which is about 10% of the mean amplitude of S_a at these stations. The sources of this systematic bias have not yet been identified. However, it is most likely that this bias can be explained by the absence of the S_a constituent

in the loading tide of equation (1). Recent investigations [Ray, 1998; Stepanov and Hughes, 2004] have shown that the displacements of loading tides have magnitudes of about 12% of the ocean tides in the deep ocean. Since the spatial scale of the S_a constituent is large in the study area (Figure 7), we may assume that the coefficient 12% can be used for rough estimation of the magnitude of the loading effect of S_a . The mean value of the amplitudes at the stations listed in Table 6 is 20 cm, while the atmospheric pressure for the study area has an annual variation with amplitudes around 7 hPa and has approximately opposite phases to the S_a tide. Thus the combined area mean load of the water column and the atmospheric pressure is about 13 hPa. By applying the coefficient of 0.12 the S_a loading tide is estimated to have amplitudes around 1.6 cm. This estimate, though very rough, is consistent with the mean discrepancy, 1.9 cm. Therefore this systematic bias might indicate the

Table 6. Comparison Between TP-Measured and Ground-Measured Annual Harmonics (S_a Constituent)^a

	Station	N/E	Duration, years	H/g(gr)	H/g(TP)	$\Delta H/\Delta g$
L1	Haiyangdao	39.07/123.15	5	21.9/126.4	21.8/130.0	−0.1/3.6
L2	Qinhuangdao	39.92/119.62	21	29.0/122.7	26.0/122.0	−3.0/−0.7
L3	Tanggu	39.10/117.72	14	31.2/121.1	27.5/126.0	−3.7/4.9
L4	Yantai	37.53/121.40	5	24.6/128.1	20.9/128.0	−3.7/−0.1
L5	Qianliyan	36.27/121.38	5	21.3/136.2	20.1/130.0	−1.2/−6.2
L6	Lusi	32.13/121.62	16	18.9/148.5	16.7/149.0	−2.2/0.5
L7	Luhuashan	30.78/122.62	19	17.2/150.9	14.9/146.0	−2.3/−4.9
L8	Kanmen	28.08/121.28	16	12.8/177.9	11.1/172.0	−1.7/−5.9
L9	Pingtan	25.45/119.98	4	10.6/208.4	8.1/201.0	−2.5/−7.4
L10	Mokpo	34.78/126.38	23	17.1/142.3	15.0/143.0	−2.1/0.7
L11	Pusan	35.10/129.03	19	11.5/143.3	12.4/150.0	0.9/6.7
L12	Naze	28.38/129.50	28	16.9/140.2	16.3/135.0	−0.6/−5.2
L13	Naha	26.22/127.67	27	14.1/144.9	12.4/135.0	−1.7/−9.9
RMS				20.0/−	18.1/−	2.2/5.3

^aDuration refers to the record length of ground measurement; $\Delta H = H(TP) - H(gr)$; $\Delta g = g(TP) - g(gr)$.

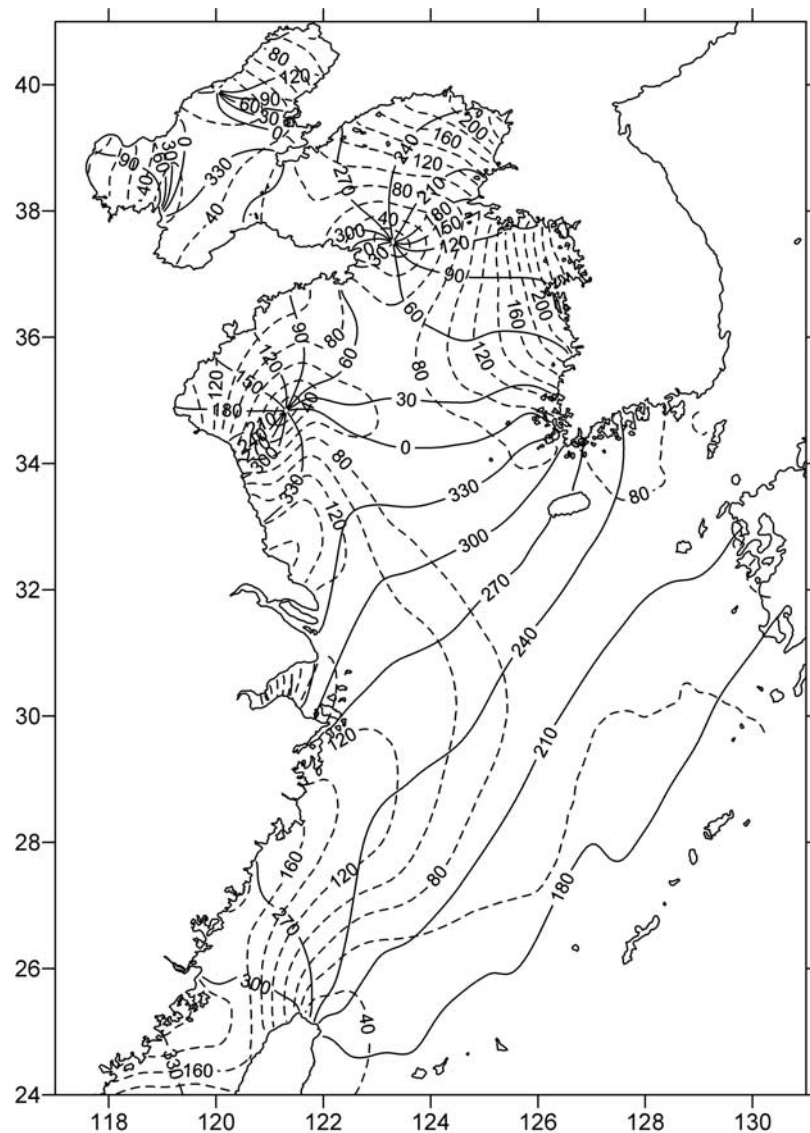


Figure 3. M_2 cotidal chart based on TP solution and coastal gauge measurements. Solid and dashed lines show distributions of phase lag (in degrees and referred to the Beijing standard time (UT + 8 hours)) and amplitude (in centimeters), respectively.

importance of the loading effect of the S_a constituent, which is so far not taken into consideration in geodetic surveys.

4. Cotidal Charts

[16] The comparisons conducted in the preceding sections indicate that the TP derived harmonic constants in the study area are in good agreement with the ground measurements for the principal constituents. The discrepancies in amplitudes are in the range 2–4 cm for M_2 and S_2 , and around 2 cm for K_1 , O_1 and S_a . The discrepancies in phase lags are mostly around 5° . Thus the TP results are adequate for constructing reliable cotidal charts for these five constituents, though they are still not as accurate as in the deep oceans [Shum *et al.*, 1997].

[17] Since the satellite altimeters are not capable of measuring sea surface heights in the nearshore areas, to construct complete cotidal charts for the area, harmonic

constants at 275 coastal and island stations, indicated by crosses in Figure 2, and TP subsatellite points are used in this study. For convenience, these stations and points are hereafter called data points. The distributions of tides in the study area are obtained through interpolation from the harmonic constants at the data points onto a uniform grid of $5'$ by $5'$. The interpolation is performed on a coordinate system with its axes along the TP subsatellite tracks. That is, we introduce an (x, y) coordinate system in which the ascending tracks 1, 77, 153, 229, 51, 127, 203 and 25 (Figure 2. The track 1 is located immediately northwest of the track 77, not shown in the figure) are assigned an x coordinate 0, 1, 2, 3, 4, 5, 6 and 7, respectively; and the descending tracks 88, 164, 240, 62, 138, 214 and 36 are assigned a y coordinate 0, 1, 2, 3, 4, 5 and 6, respectively. This system can be called TP track coordinate system. The relationship between the TP track coordinates (x, y) and the geographic coordinates (λ, φ) in the study area can be

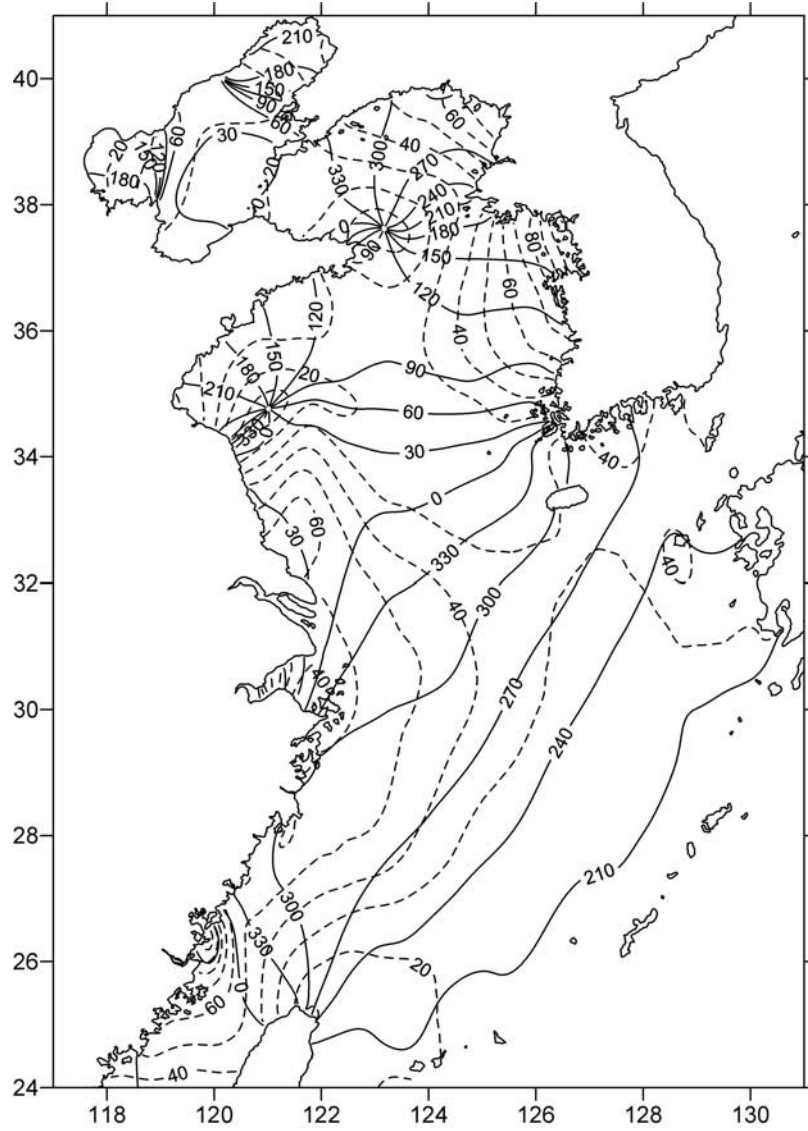


Figure 4. Same as Figure 3, but for S_2 .

derived from the geographic coordinates of the crossover points as follows:

$$\begin{cases} \lambda = a_1 + a_2(x + y), \\ \varphi = a_3 + a_4(y - x) + a_5(y - x)^2, \end{cases} \quad (9)$$

where λ , φ and $a_i (i = 1, 2, \dots, 5)$ are given in degrees, with $a_1 = 113.386$, $a_2 = 1.4173$, $a_3 = 32.370$, $a_4 = 2.5617$, $a_5 = 0.092777$. If the geographic coordinates (λ, φ) are known, the values of $x + y$ and $y - x$ can be inversely calculated from (9), and the coordinates (x, y) can then be obtained. Thus the geographic coordinates of all data points and grid points are converted into TP track coordinates through relationship (9). At the data points the harmonic constants H and g are converted to the cosine component $H \cos g$ and the sine component $H \sin g$. In the following we will use a variable z to represent either cosine or sine component of a constituent.

[18] The value of z at a grid point (x_n, y_n) is then interpolated from the results at its surrounding data points within the influence distance r , which is taken to be 1.1 in

order to cover at least 2 tracks. Since the spatial scales of the tidal waves in shelf seas are not long enough in comparison to the spacing of the subsatellite tracks, a linear interpolation will induce noticeable error. Here we adopt the locally weighted quadratic polynomials to fit the data. The method is similar to that presented by *Ridgway and Dunn* [2002], but in our case two dimensions are involved.

[19] Suppose there are K data points within the influence distance of a grid point (x_n, y_n) . The following interpolating function is fitted to the variable z at each of these points:

$$\begin{aligned} \hat{z}_k = & b_1 + b_2 \Delta x_k + b_3 \Delta y_k + b_4 \Delta x_k^2 \\ & + b_5 \Delta x_k \Delta y_k + b_6 \Delta y_k^2, \quad (k = 1, 2, \dots, K) \end{aligned} \quad (10)$$

where $\Delta x_k = x_k - x_n$, $\Delta y_k = y_k - y_n$, with x_k and y_k representing the TP track coordinates of the k th data point. The equations are weighted with an exponential function

$$w_k = \exp(-r_k/l), \quad (11)$$

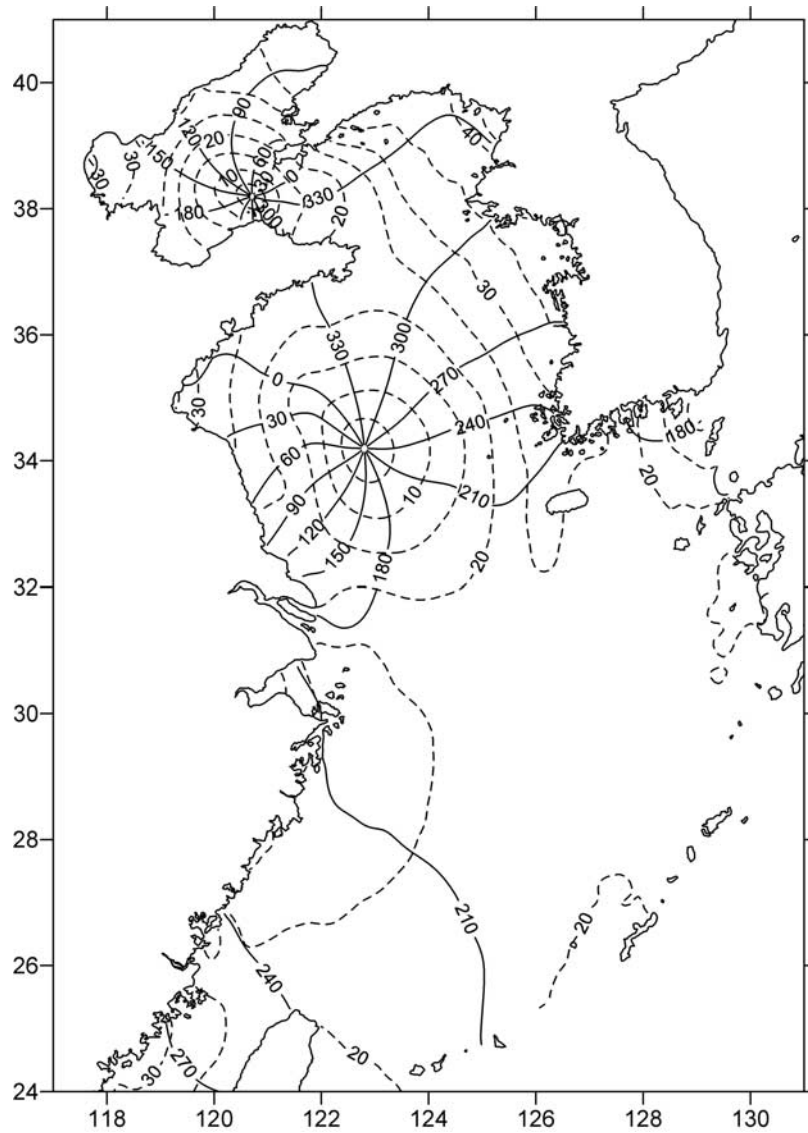


Figure 5. Same as Figure 3, but for K_1 .

where $r_k = (\Delta x_k^2 + \Delta y_k^2)^{1/2}$, l is an adjustable length scale ranging from 0.3 in inshore area to 1.0 in offshore area. This yields an over determined set of algebraic equations:

$$MB = Z, \quad (12)$$

where

$$B = (b_1, b_2, \dots, b_6),$$

$$Z = (z_1, z_2, \dots, z_K),$$

$$M = \begin{bmatrix} w_1 & w_1 \Delta x_1 & w_1 \Delta y_1 & w_1 \Delta x_1^2 & w_1 \Delta x_1 \Delta y_1 & w_1 \Delta y_1^2 \\ w_2 & w_2 \Delta x_2 & w_2 \Delta y_2 & w_2 \Delta x_2^2 & w_2 \Delta x_2 \Delta y_2 & w_2 \Delta y_2^2 \\ \dots & \dots & \dots & \dots & \dots & \dots \\ w_K & w_K \Delta x_K & w_K \Delta y_K & w_K \Delta x_K^2 & w_K \Delta x_K \Delta y_K & w_K \Delta y_K^2 \end{bmatrix}.$$

Applying least squares fit leads to the corresponding normal equation

$$(M^T M)B = M^T Z, \quad (13)$$

in which T denotes a transpose. Equation (13) can be readily solved. The estimate of \hat{z} at (x_n, y_n) is equal to b_1 .

[20] The derived cotidal charts for M_2 , S_2 , K_1 , O_1 and S_a are given in Figures 3–7. Though the cotidal charts derived from TP altimetry and ground observations in the present study have similar patterns to those obtained in the previous studies, a careful inspection can find many subtle differences, due to improved accuracy of the present charts. It is most obvious that the positions of amphidromic points given in the previous studies generally differ to a certain degree from the present results.

[21] In most previous studies the positions of amphidromic points were determined on the basis of coastal

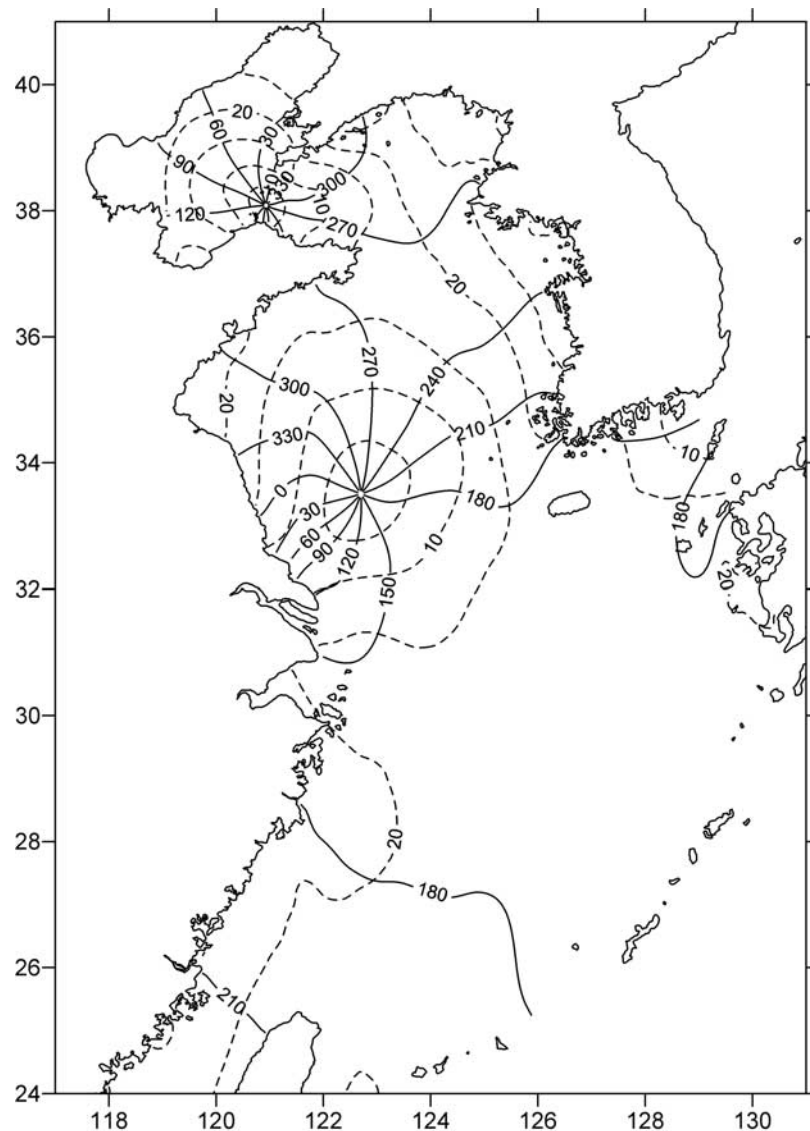


Figure 6. Same as Figure 3, but for O_1 .

observations or numerical simulations. In this study, the harmonic constants along the TP tracks have been used, leading to higher accuracy in the positions of amphidromic points, which are listed in Table 7.

[22] Figures 3 and 4 show that both the M_2 and S_2 tides have three amphidromic points: one in the Bohai Sea and two in the Yellow Sea. The amphidromic points in the Bohai Sea are very close to the coast near Qinhuangdao (Figure 1). Near the Yellow River mouth the amphidromes appear as degenerated systems. The amphidromic points of the semidiurnal tides in the Yellow Sea are located northeast of Chengshantou and southeast of Qingdao, respectively (Figure 1). In comparison with the M_2 tide, the amphidromic points of S_2 in the Yellow Sea are shifted inward and leftward if the observer faces toward the closed end of the sea. The inward shift is due to shorter wavelength of S_2 than M_2 . The leftward shift is a result of nonlinearity of the bottom friction, which causes the smaller waves to suffer a greater attenuation [Fang, 1987].

[23] Figures 5 and 6 show that the K_1 and O_1 have two amphidromic points: one located in the Bohai Strait and another in the Southern Yellow Sea. Both O_1 amphidromic points have outward displacements relative to the corresponding K_1 amphidromic points due to longer wavelength. The frictional nonlinearity causes the O_1 amphidromic points to have leftward displacements relative to the corresponding K_1 amphidromic points. As a consequence, the amplitude ratios O_1/K_1 along the western shore of the Southern Yellow Sea are generally significantly smaller than those along the eastern shore. For example, the ratio is equal to 0.51 at Lusi and is 0.79 at Mokpo (Figure 1).

[24] The meteorological tide S_a does not show amphidromic system in the study area (Figure 7). Its amplitude is larger in the north and smaller in the south, reflecting the action of monsoon forcing. Moreover, the amplitude varies much greater in the Bohai Sea and northern Yellow Sea because of shallowness of this area in comparison to the southern Yellow Sea and northern East China Sea. The

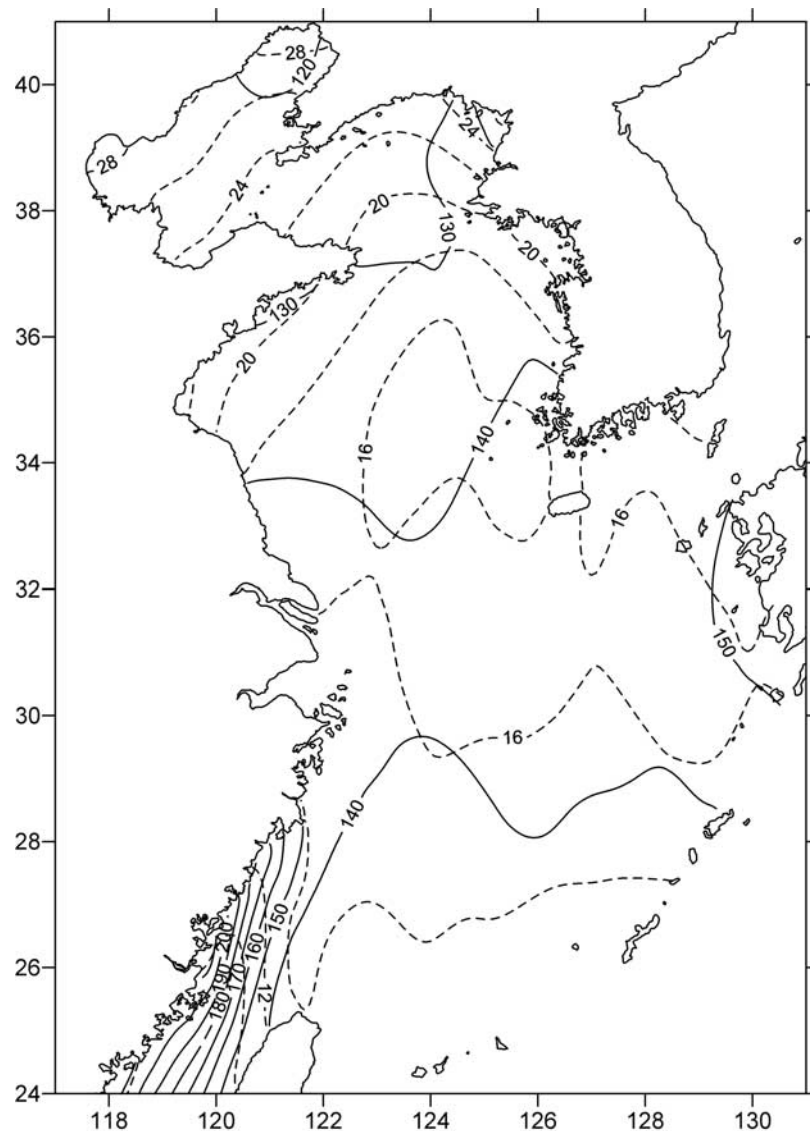


Figure 7. Same as Figure 3, but for S_a .

phase lag changes rapidly around the Taiwan Strait. This is a result of monsoon induced sea level variation in the strait and remarkable difference in seasonal sea level variations between the East China Sea and the South China Sea.

5. Discussion and Conclusion

[25] The intercomparison between the harmonics of ascending and descending tracks at crossover points in the study area shows typical RMS differences smaller than 4 cm for M_2 and S_2 and around 2 cm for the rest constituents.

[26] The RMS differences of amplitude and phase of 4 principal constituents between TP solutions and the ground measurements at islands are around 2 cm and 5° , respectively. The corresponding differences between TP solutions and ground measurements in the open sea are in the range of 1.4–4.8 cm and 7° – 11° , respectively. The larger differences between TP and open sea results than those between TP and island results can be attributed to the

lower accuracy of the open sea results, mainly because of the difficulty in operation of in situ observations.

[27] From the crossover and TP-ground comparisons we can estimate that the accuracy of the harmonics in the study area derived from 10 years of TP altimetry has achieved a level of 2–4 cm for M_2 and S_2 amplitudes, a level of 2 cm for the amplitudes of the other constituents, and a level of 5° for phase lags of principal constituents (M_2 , S_2 , K_1 , O_1 and S_a). Though the TP-derived harmonic constants in this shallow area are not as accurate as in deep oceans [Shum *et al.*, 1997], they are very valuable in determining the tides

Table 7. Position of Amphidromic Points From the Present Study

	M_2	S_2	K_1	O_1
1	39°55'/120°01'	40°00'/120°10'	38°11'/120°42'	38°04'/120°55'
2	37°30'/123°18'	37°37'/123°10'	34°12'/122°48'	33°30'/122°42'
3	34°50'/121°18'	34°46'/121°01'		

in the offshore area. Cotidal charts produced from the present study are more reliable than the previous charts.

[28] The present study also reveals that for nonprincipal astronomical constituents the errors in TP solutions are comparable or even greater than the magnitudes of these constituents themselves when the least squares fit is directly utilized in the analysis. To reduce the errors in these constituents, one may infer their amplitudes and phase lags from principal constituents, or apply the response method to the analysis with small lag integer K as done by *Cartwright and Ray* [1990]. The nonprincipal meteorological tides, such as S_{sa} , and shallow water tides, such as M_4 , MS_4 , M_6 , etc. cannot yet be detected by TP measurement to a sufficient accuracy for the study area, except that TP-derived M_4 is of certain significance in some individual areas, where M_4 is relatively large.

[29] The TP solution of S_a constituent is likely to have a systematic bias toward lower values by about 10%. Our rough estimation shows that this bias could possibly be attributed to the loading effect, indicating the importance of loading effect of this constituent on the seas of the present study and the nearby land area, which is so far not considered in geodetic surveys.

[30] **Acknowledgments.** The altimetry data used in the present study were obtained from the NASA Physical Oceanography Distributed Active Archive Center at the Jet Propulsion Laboratory/California Institute of Technology. Comments given by the reviewers greatly improved the manuscript. The present study was supported by the National Natural Science Foundation of China under grant 40076004, and National Science and Technology Special Program under grant 03010105.

References

- Benada, J. R. (1997), *Merged GDR (TOPEX/POSEIDON), Generation B, User's Handbook*, 124 pp., Jet Propul. Lab., Calif. Inst. of Technol., Pasadena.
- Cartwright, D. E., and R. D. Ray (1990), Oceanic tides from Geosat altimetry, *J. Geophys. Res.*, **95**, 3069–3090.
- Choi, B. H. (1980), A tidal model of the Yellow Sea and the Eastern China Sea, *KORDI Rep. 80-2*, Korea Ocean Res. and Dev. Inst., Ansan.
- Choi, B. H. (1983), Analysis of mean sea levels and tides for major ports of Korea (in Korean), *Natl. Geogr. Inst. Rep.*, 332 pp., Seoul, Korea.
- Choi, B. H., and G. Fang (1993), A review of tidal models for the East China and Yellow Seas, *J. Korean Soc. Coastal Ocean Eng.*, **5**, 151–171.
- Fang, G. (1986), Tide and tidal current charts for the marginal seas adjacent to China, *Chin. J. Oceanol. Limnol.*, **4**, 1–16.
- Fang, G. (1987), Nonlinear effects of tidal friction, *Acta Oceanol. Sin.*, **6**, suppl. 1, 105–122.
- Fang, G., and J. Yang (1985), A two-dimensional numerical model of the tidal motions in the Bohai Sea, *Chin. J. Oceanol. Limnol.*, **3**, 135–152.
- Fang, G., W. Zheng, Z. Chen, and J. Wang (1986), *Analysis and Prediction of Tides and Tidal Currents* (in Chinese), 474 pp., China Ocean, Beijing, China.
- Foreman, M. G. G. (1977), Manual for tidal analysis and prediction, *Pac. Mar. Sci. Dep. 77-10*, 66 pp., Inst. Ocean Sci., Sidney, B. C., Canada.
- Fu, L.-L., E. J. Christensen, C. A. Yamarone Jr., M. Lefebvre, Y. Ménard, M. Dorner, and P. Escudier (1994), TOPEX/Poseidon mission overview, *J. Geophys. Res.*, **99**, 24,369–24,381.
- Godin, G. (1972), *The Analysis of Tides*, 264 pp., Univ. Toronto Press, Toronto, Ontario, Canada.
- Kang, S., K. S.-R. Lee, and H.-J. Lie (1998), Fine grid tidal modeling of the Yellow and East China Seas, *Cont. Shelf Res.*, **18**, 739–772.
- Lee, J. C., and K. T. Jung (1999), Application of eddy viscosity closure models for the M2 tide and tidal currents in the Yellow Sea and the East China Sea, *Cont. Shelf Res.*, **19**, 445–475.
- Lefebvre, F., C. Le Provost, and F. H. Lyard (2000), How can we improve a global ocean tide model at a regional scale? A test on the Yellow Sea and the East China Sea, *J. Geophys. Res.*, **105**, 8707–8725.
- Mazzega, P., and M. Berge (1994), Ocean tides in Asian semiencloded seas from TOPEX/Poseidon, *J. Geophys. Res.*, **99**, 24,867–24,881.
- Munk, W., B. Zetler, and G. Groves (1965), Tidal cusps, *Geophys. J.*, **10**, 211–219.
- Ogura, S. (1933), The tides in the seas adjacent to Japan, *Bull. Hydrogr. Dep. 7*, 198 pp., Imperial Jpn. Navy, Tokyo.
- Pawlowicz, R., B. Beardsley, and S. Lentz (2002), Classical tidal harmonic analysis including error estimates in MATLAB using T_TIDE, *Comput. Geosci.*, **28**, 929–937.
- Ray, R. D. (1998), Ocean self-attraction and loading in numerical tidal models, *Mar. Geod.*, **21**, 181–192.
- Ridgway, K. R., and J. R. Dunn (2002), Ocean interpolation by four-dimensional weighted least squares-application to the waters around Australasia, *J. Atmos. Oceanic Technol.*, **19**, 1357–1375.
- Schlag, M. G., and D. B. Chelton (1994), Aliased tidal errors in TOPEX/Poseidon sea surface height data, *J. Geophys. Res.*, **99**, 24,761–24,775.
- Shum, C. K., et al. (1997), Accuracy assessment of recent ocean tide models, *J. Geophys. Res.*, **102**, 25,173–25,194.
- Stepanov, V. N., and C. W. Hughes (2004), Parameterization of ocean shelf-attraction and loading in numerical models of the ocean circulation, *J. Geophys. Res.*, **109**, C03037, doi:10.1029/2003JC002034.
- Teague, W. J., H. T. Perkins, Z. R. Hallock, and G. A. Jacobs (1998), Current and tide observations in the southern Yellow Sea, *J. Geophys. Res.*, **103**, 27,783–27,793.
- Teague, W. J., P. Pistek, G. A. Jacobs, and H. T. Perkins (2000), Evaluation of tides from TOPEX/Poseidon in the Bohai and Yellow Seas, *J. Atmos. Oceanic Technol.*, **17**, 679–687.
- Yanagi, T., A. Morimoto, and K. Ichikawa (1997), Co-tidal and co-range charts for the East China Sea and the Yellow Sea derived from satellite altimetric data, *J. Oceanogr.*, **53**, 303–309.
- Zhao, B., G. Fang, and D. Cao (1993), Numerical modeling on the tides and tidal currents in the Eastern China Sea, *Yellow Sea Res.*, **5**, 41–61.
- B. H. Choi, Department of Civil and Environment Engineering, Sungkyunkwan University, 300 Suwon, 440-746 Korea.
- G. Fang, X. Wang, Y. Wang, and Z. Wei, First Institute of Oceanography, State Oceanic Administration, Qingdao, 266061 China. (fanggh@fil.org.cn)
- J. Wang, National Marine Data and Information Service, Tianjin, 300171 China.